ACS Catalysis

Research Article

Cite This: ACS Catal. 2019, 9, 3527−3536

pubs.acs.org/acscatalysis

Suppressing H_2 Evolution and Promoting Selective CO_2 Electroreduction to CO at Low Overpotentials by Alloying Au with Pd

Marco Valenti,*[,†] Nitin P. Prasad,[†] Recep Kas,[†] Divya Bohra,[†] Ming Ma,[†] Vignesh Balasubramanian,[†] Liangyong Chu,[†] Sixto Gimenez,[‡] Juan Bisquert,[‡] Bernard Dam,[†] and Wilson A. Smith*[,†]

[†]Materials for Energy Conversion and Storage (MECS), Department of Chemical Engineering, Delft University of Technology, Delft 2629 HZ, The Netherlands

[‡]Photovoltaic and Optoelectronics Devices Group, Departament de Fisica, Universitat Jaume I Av Sos Baynat s/n, 12071 Castello, Spain

Supporting Information

ABSTRACT: CO_2 electroreduction is a promising technology to produce chemicals and fuels from renewable resources. Polycrystalline and nanostructured metals have been tested extensively while less effort has been spent on understanding the performance of bimetallic alloys. In this work, we study compositionally variant, smooth Au−Pd thin film alloys to discard any morphological or mesoscopic effect on the electrocatalytic performance. We find that the onset potential of CO formation exhibits a strong dependence on the Pd content of the alloys. Strikingly, palladium, a hydrogen evolution catalyst with reasonable exchange current density, suppresses hydrogen evolution when alloyed with gold in the presence of CO_2. Cyclic voltammetry, in situ surface enhanced infrared absorption spectroscopy, and potential-dependent online product analysis strongly suggest that by alloying Au with Pd a significant increase in the surface coverage of adsorbed CO occurs with increasing Pd content at low overpotentials (e.g., approximately −0.35 V vs RHE). Such an increase in CO coverage suppresses H_2 evolution due to the lack of vacant active sites. Moreover, the overall increase in the binding energy with the CO_2 intermediates gained with the addition of Pd increases the CO production at low overpotentials, where polycrystalline Au suffers from poor CO_2 adsorption and poor selectivity for CO production. These results show that promising CO_2 reduction electrode materials (e.g., Au) can be alloyed not only to tune the catalyst's activity but also to deliberately decrease the availability of surface sites for competitive H_2 evolution.

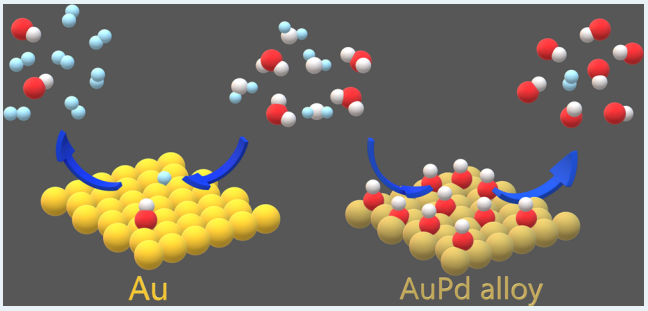

KEYWORDS: *electrochemical CO_2 reduction, in situ spectroelectrochemistry, hydrogen suppression, metallic alloy thin films, kinetic modeling*

INTRODUCTION

Over the past few decades, the electrochemical reduction of CO_2 has attracted increasing interest because of its potential to help close the anthropogenic carbon cycle, while also providing a promising route to store intermittent renewable electricity in chemical bonds.[1] Chemicals and fuels produced from CO_2 allow for a smooth and easy transition toward a renewable energy economy, which could also be readily implemented in the current energy infrastructure.[2] Even though CO_2 electroreduction can produce a wide range of products, some major challenges must be addressed before it becomes appealing for large-scale applications. These include poor product selectivity, the need for high overpotentials, and low faradaic and energy efficiencies.[3−7]

In aqueous electrolytes, the CO_2 electroreduction reaction competes in selectivity with the hydrogen evolution reaction. For improved energy-efficient devices, which require a low operating voltage, it is of particular importance to control this competition at low overpotentials. In fact, Hori et al.[8] found that most metals preferentially produce hydrogen under reducing conditions, even in the presence of CO_2. Systematic studies that aim to understand the effect of the electrode's morphology[9,10] and electronic properties (with bimetallic alloys)[2,11−13] provide insights into the elementary mechanisms taking place in the reduction of CO_2 and H_2O. Understanding these mechanisms can allow the ability to control the ratio between H_2 evolution and CO formation to meet the needs of industrial applications (e.g., Fischer−Tropsch synthesis), while keeping the overall device energy-efficient.

Received: November 16, 2018
Revised: March 4, 2019
Published: March 11, 2019

DOI: 10.1021/acscatal.8b04604
ACS Catal. 2019, 9, 3527−3536

Group 11 metals of the periodic table, Cu, Ag, and Au, have been extensively studied as electrocatalysts for the CO_2 reduction reaction (CO2RR).[14] Au has been shown to be the most selective and active catalyst to convert CO_2 to CO.[8,14,15] This is mainly due to the relatively favorable binding energies of the CO_2 intermediates (i.e., COOH and CO) for the conversion to CO on Au.[9] However, at low overpotentials (approximately <0.5 and <0.3 V vs RHE for polycrystalline Au and oxide-derived Au nanoparticles, respectively[16]), the H_2 evolution reaction (HER) compromises the selectivity for CO. The selectivity of the catalyst toward CO could be improved by suppressing the HER.[17] It has been observed that Pd strongly adsorbs CO2RR intermediates at low overpotentials, covering the electrode surface and decreasing the availability of sites for the HER.[18] This phenomenon was shown[18] with Pd nanoparticles that effectively evolve H_2 at low overpotentials when purging the electrolyte with Ar, while in the presence of CO_2 the currents for H_2 evolution would be significantly reduced due to the strong adsorption of CO2RR species (e.g., CO) on the electrode surface. Such strong CO2RR intermediate species adsorption and high CO_2 intermediate coverages of Pd are in good agreement with density functional theory (DFT) calculations[17,19,20] and several experimental works.[21−23] Even though the HER is suppressed on Pd, the CO binding energy is too strong for an efficient release of the product.

The binding energies between the electrode and intermediate species for the CO2RR and HER directly affect (i) the competition for active surface sites during the adsorption process of the corresponding reactants (CO_2 and H_2O/H^+ for the CO2RR and HER, respectively[17]) and (ii) the activity of the catalyst for the respective reactions.[17] The binding energy in transition metals depends on the interaction between the valence band of the metal (i.e., d-band and s-band) and the specific valence state of the intermediate.[24] In general, it has been shown that the closer the d-band is to the Fermi level of the metal, the larger is the binding energy with intermediates.[24] For instance, Au has the d-band ∼2.3 eV below its Fermi level and interacts relatively weakly with the intermediates when compared with Pd, which has a d-band that partially overlaps with the Fermi level.

Alloying Au with different concentrations of Pd allows the ability to controllably shift the d-band closer to the Fermi level, which increases the binding energies with reaction intermediates.[25] As mentioned earlier, the binding energies affect the adsorption process, and it is expected that metals with relatively large binding energies (e.g., Pd) can stabilize adsorbed intermediates more efficiently, resulting in larger adsorbate coverages at lower overpotentials. Alloying Au with Pd can increase the coverage of CO2RR species due to an increase in binding energies. Therefore, the large CO2RR intermediate species coverages found in Pd that limit the HER sites could also be expected to a certain extent in the Au−Pd alloy. However, changing the binding energy of Au by alloying with Pd will affect not only the competition for sites for the two competing reactions but also the activity of the catalyst toward the two reactions. This way, while the effect of limiting the HER sites by alloying Au with Pd could promote CO formation (through more active sites), the kinetics of the reaction may be compromised by less optimal binding energies for CO formation. This communication aims to experimentally study the effect of these two counteracting effects during CO2RR on Au−Pd alloys, in an attempt to understand the selectivity of Au toward CO at low overpotentials. The electrocatalytic performance of Au−Pd alloys has already been studied at high potentials focusing on the formation of hydrocarbons[26] and formic acid.[27] Here, we focus our investigation on the selectivity to CO and hydrogen at low potentials by using compositionally variant Au−Pd thin film alloys.

RESULTS

Magnetron cosputtering was used to deposit thin films of 5 different compositions (Au, $Au_{75}Pd_{25}$, $Au_{50}Pd_{50}$, $Au_{25}Pd_{75}$, and Pd) on Ti foils. The morphology of the electrodes has been proven to play an important role in the CO2RR.[9,28,29] Because this work aims to exclusively study the electronic/compositional effects of the synthesized electrodes on the CO2RR, it is necessary to have the morphology of the thin film alloys be nearly the same. RMS roughness calculated from atomic force microscopy (AFM) confirms that all alloys were equally flat with a roughness of ∼2 nm (see Figure 1S in the Supporting Information SI-1).

X-ray photoelectron spectroscopy (XPS) measurements were carried out to study the electronic/compositional properties of the electrodes surface, which can provide insights into the binding energy of the intermediates on the catalyst surface. Figure 1 shows the valence band spectra of the electrodes with different compositions. The peaks in the XPS spectra correspond to the d-band of the metals, which strongly interacts with the reaction intermediate species.[2] The closer the d-band is to the Fermi level, here normalized to 0 eV, the larger are the binding energies of the metal with all the intermediates.[30] From Figure 1, it can be seen that, with increasing Pd content, the d-band shifts closer to the Fermi level, allowing the electrode to interact to a larger extent with CO2RR and HER intermediates. To ensure that the materials retain their surface electronic structure during CO_2 reduction, the XPS spectra were collected before (solid lines) and after electrolysis (dashed lines) at −0.5 V vs RHE for 20 min. No significant changes in the shape of the valence band are noted, which suggests that no phase segregation occurred during the reaction that could affect the local electronic properties of the electrode surface. It is important to highlight that the penetration depth of the XPS measurement shown in Figure 1 is ∼3 nm. Reske et al.[31] observed that the electronic properties of the materials ∼10 nm under the top monolayer (in direct contact with the intermediates) also significantly affect the CO2RR. XPS spectra of the valence band were measured after 29 cycles of etching (see Supporting Information SI-2), and still no significant changes were observed. Therefore, the XPS measurements shown in Figure 1 are a good approximation to the actual electronic properties and surface composition affecting the reaction. While the compositions shown in the labels of Figure 1 are the ideal compositions expected after sputtering, a measurement of the composition was done using the Au $4p_{3/2}$ and Pd $3d_{3/2}$ peaks in the XPS survey spectrum, and a difference of ∼5−7% was observed for the compositions indicated in Figure 1 (see Supporting Information SI-3).

The XPS measurements give a clear average of the electronic properties of the alloys. However, it is also important to get information on the homogeneity of the alloy on the electrode surface. To observe this, cyclic voltammetry[32] (CV) was carried out in 0.1 M sulfuric acid in order to study the distinctive reduction peaks of the pure and alloyed metallic

DOI: 10.1021/acscatal.8b04604
ACS Catal. 2019, 9, 3527−3536

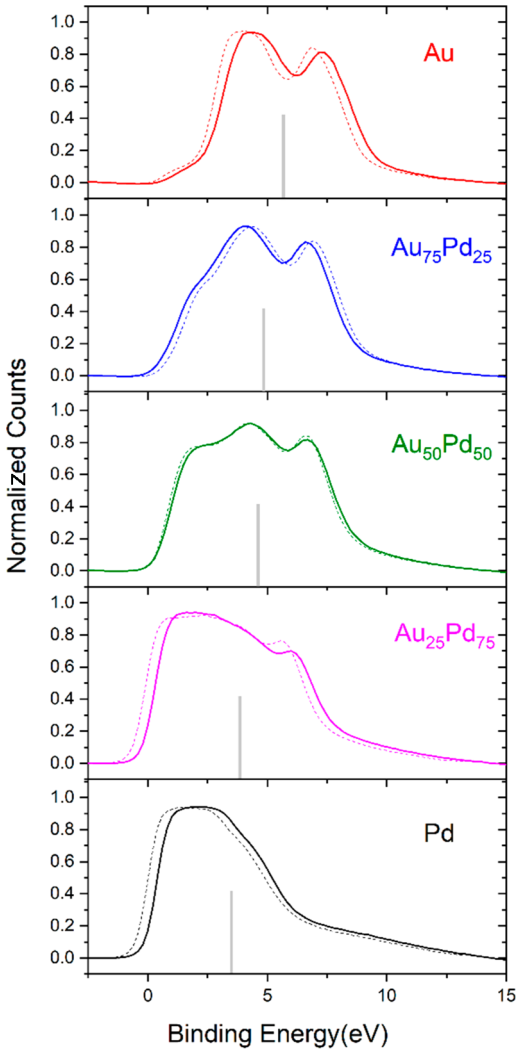

Figure 1. XPS valence band spectra of Au, Pd, and Pd−Au alloys films before CO_2 reduction (solid line) and after CO_2 reduction (dashed line). The position of the d-band center of Au−Pd bimetallic films (gray vertical lines) is observed to shift closer to the Fermi level with increasing Pd content in the alloys.

electrodes from their oxide states. Figure 2 shows the CV sweeps for each composition. All the cyclic voltammograms in Figure 2 start with an anodic sweep, and the resulting anodic currents correspond to the oxidation of the metals, metal dissolution (e.g., ∼5% for Pd[33]), and O_2 evolution for the Pd-rich electrodes. On the other hand, the cathodic current peaks correspond exclusively to the reduction of the metal oxides to their metallic state, and their position in the CV spectrum can give information on the electrode's composition. The characteristic reduction peaks of Pd and Au appear at ∼0.5 V vs RHE and ∼1.1 V vs RHE, respectively, which is consistent with other studies.[34] The reduction peaks for all the alloys are located in between the peaks of the pure components, which is characteristic for bimetallic alloys.[35,36] A key observation is that none of the reduction peaks of the alloys overlap with the pure components, which indicates that there are no regions on the alloy electrode surfaces with pure Au or Pd. This is in good agreement with the fact that Au and Pd can form face-centered cubic (FCC) alloys over the entire composition range.[37] Clearly, the alloy peaks shift to more positive potentials with increasing Au content. However, more than one peak can be

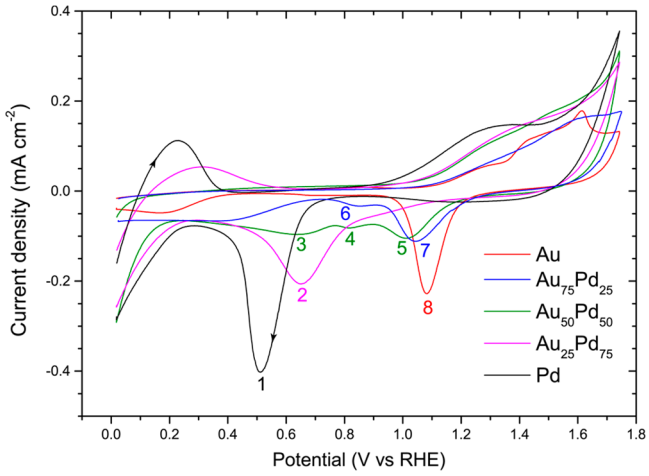

Figure 2. CV of Au−Pd thin-film alloys used for the qualitative characterization of the surface composition of thin films in 0.1 M H_2SO_4 (pH = 0.77) with a scan rate of 50 mV s^{-1} in the potential range 0−1.7 V. Each cycle starts with an anodic scan from 0 to 1.7 V followed by a cathodic scan. The direction of the scan is shown in the CV for pure Pd (black).

identified for the alloys with 50% and 75% Au, indicating that there are different regions with different alloy compositions on the surface of the electrodes. The alloy peaks are expected to move linearly with composition between the peaks of the pure metals.[36] For the alloy with 25% Au, a Pd-rich alloy peak is more prominent (peak 2 in the figure), while for the 75% Au sample, the Au-rich alloy peak (peak 7) is more prominent. For the 50% Au sample, three peaks can be seen with similar intensities, with one in the middle of the two pure peaks (peak 4) that corresponds to a ∼50−50 alloy region and the other two that correspond to Pd-rich (peak 3) and Au-rich (peak 5) alloy regions. Therefore, the CO2RR results shown below correspond to these different alloy regions and not to a single alloy composition.

It is worth highlighting that precisely three reduction peaks were found in the synthesized 50% Au alloy. Au and Pd have been reported to exist in three metastable phases with superstructures for $AuPd_3$, Au_3Pd (already identified), and the equiatomic composition (yet to be ascertained).[38] Therefore, the three different reduction peaks found in the electrode may correspond to the preferential formation of these three superstructures on the electrode's surface.

The electrodes were tested as electrocathodes in an electrochemical cell with a Nafion membrane placed in between the cathode and the anode (Pt flat film). The potential of the electrocathodes was controlled with a potentiostat in a three-electrode configuration, and a gas chromatograph (GC) was coupled to the cell to monitor the gas products. The faradaic efficiencies (FEs) for CO and H_2 of the 5 synthesized electrodes at −0.5 V vs RHE are shown in Figure 3 (see FE standard deviation calculation in the Supporting Information SI-4). The total FEs are nearly 100% for the compositions containing 50%, 75%, and 100% Au, while the FEs for the Pd-rich alloy and pure Pd are <50%. The missing FEs for the Pd-rich alloy and for pure Pd can be explained by the ability of Pd to absorb H, forming PdH.[37,39,40] From the synthesized alloys, H absorption is most prominent for the Pd-rich alloy and pure Pd (see cyclic voltammetry results and discussion in the Supporting Information SI-5), in good agreement with other studies on H_2 sensors[41] and the

DOI: 10.1021/acscatal.8b04604
ACS Catal. 2019, 9, 3527−3536

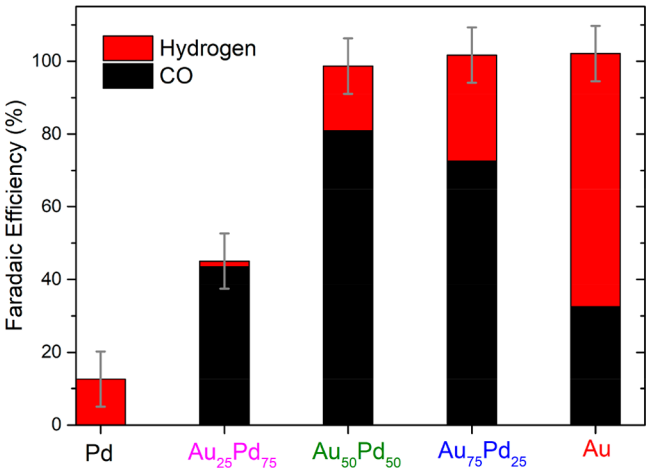

Figure 3. Faradaic efficiency of CO and H_2 for Au, Pd, and Au/Pd alloys at potentials of −0.5 V vs RHE in CO_2 saturated 0.1 M $KHCO_3$ electrolyte (pH = 6.8). The FE of CO is found to be highest for $Au_{50}Pd_{50}$. The total FE does not add up to 100% for pure Pd and $Au_{25}Pd_{75}$.

missing total FE (Figure 3). The Au-rich electrode (i.e., with 75% Au) does not show any appreciable H absorption with cyclic voltammetry (see Supporting Information SI-5), which is consistent with other electrochemical studies[37] and the measured 100% total FE in Figure 3. On the other hand, H absorption in the 50% Au electrode can occur (see Supporting Information SI-5). However, the total FE of ∼100% obtained for this sample (i.e., 50% Au) suggests that H absorption is significantly hindered during CO_2 electroreduction.

The most interesting observation of the FE shown in Figure 3 is that alloying Au with any amount of Pd increased its FE for CO, despite the fact that no CO could be measured for the pure Pd electrode. From the point of view of the activity of the alloy, this is unexpected because Au is on the right side of the volcano plot for the HER (i.e., catalysts that bind H too weakly for the HER[42]) and the addition of Pd could strengthen the interaction with the proton and therefore optimize the binding energies of Au for the HER.[43] Moreover, among the transition metals, pure Au already has a near optimal binding energy with the intermediate CO for CO formation.[20] Therefore, the addition of Pd is expected to strengthen this bond and hamper the release of CO at a high enough Pd content, making it unlikely that all the alloy compositions have more appropriate binding energies with the intermediates (i.e., COOH and CO) for the formation of CO than Au. However, the measured increase in the FE for CO in all the alloys (Figure 3) can also be explained by the competition for active sites between the CO_2 intermediates and proton adsorption.

To further study the increase in CO formation observed in Figure 3, the FEs were measured at different applied potentials (cf. Figure 4). Figure 4 shows that the alloys exhibit a larger FE for CO than pure Au for all potentials less negative than −0.65 V. The alloy electrodes and the pure Au electrode progressively increase the CO FE with increasing applied potential, which is accompanied by a corresponding decrease in the FE for H_2, suggesting a competition between the reactions. Surprisingly, the increase in the FE for CO and the corresponding decrease in the FE for H_2 occur at less negative potentials with increasing Pd content, effectively lowering the onset potential for CO formation.

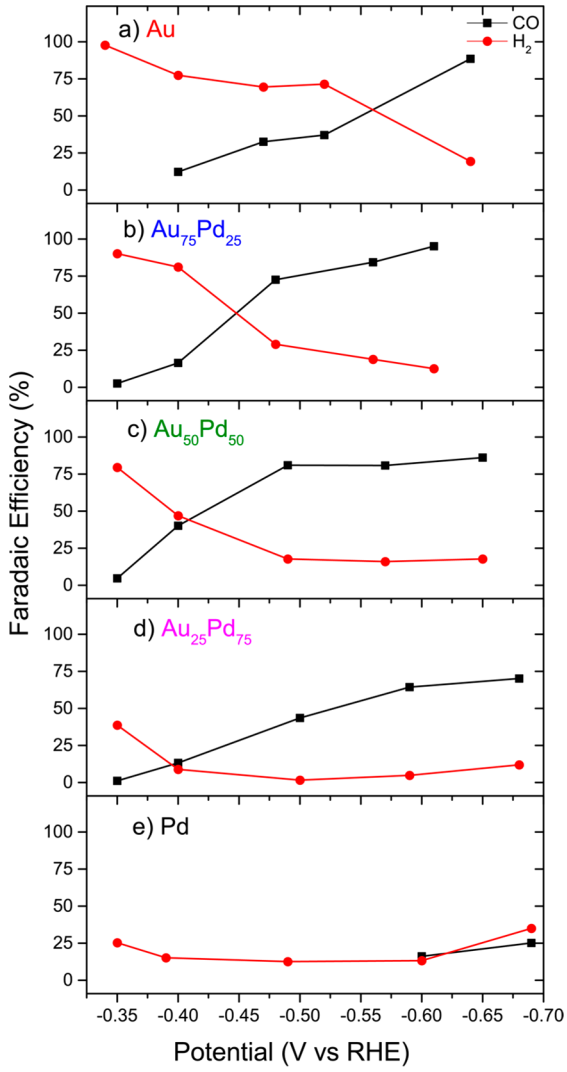

Figure 4. Faradaic efficiency of CO (black) and H_2 (red) for (a) Au, (b) $Au_{75}Pd_{25}$, (c) $Au_{50}Pd_{50}$, (d) $Au_{25}Pd_{75}$, and (e) Pd at different potentials in CO_2 saturated 0.1 M $KHCO_3$ electrolyte (pH = 6.8). No CO is formed at potentials lower than −0.6 V for Pd and −0.4 V for Au. Moreover, the FE of CO surpasses the FE of H_2 at lower potentials with increasing Pd.

To shed light on the competition between the HER and the CO2RR observed in Figure 4, the partial currents for H_2 and CO as a function of applied potential are shown in parts a and b of Figure 5, respectively. Clearly, the H_2 partial current is decreased in the alloy electrodes with increasing Pd content for all applied potentials. As explained above, a decrease in the activity for the HER with increasing Pd content is not expected. Instead this decrease in H_2 partial currents suggests that the same H_2 suppression effect found in Pd[18] in the presence of CO_2 can be occurring in the alloys. For Pd catalysts, the HER sites are limited due to the large CO2RR coverages on the electrode. If the same effect is happening on the alloy electrodes and the activity of the alloy for the competing reactions is not affected significantly, an increase in the CO partial current can be expected in the alloy due to the increased CO2RR active sites. This is in good agreement with the increase in CO partial current for the Au-rich alloy, which exhibits larger CO partial currents than Au for all applied potentials (Figure 5b). The decrease in CO partial current

DOI: 10.1021/acscatal.8b04604
ACS Catal. 2019, 9, 3527−3536

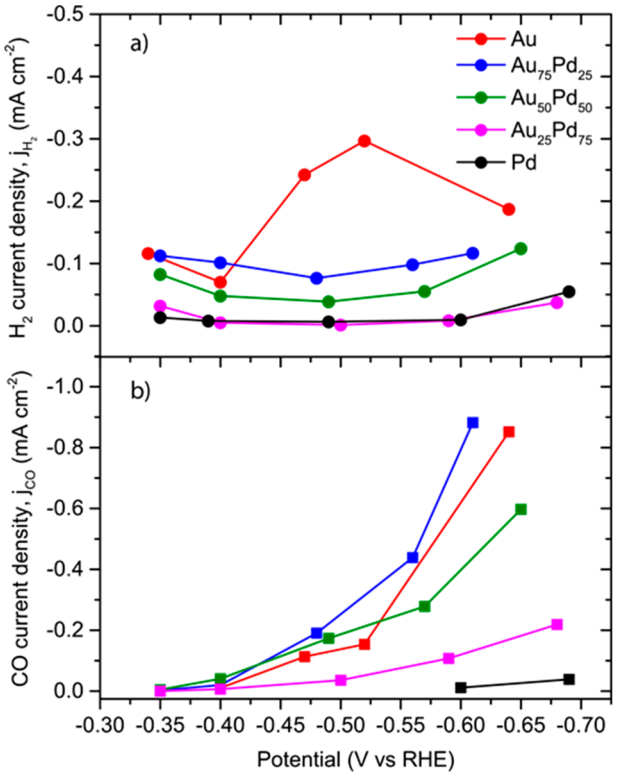

Figure 5. Partial current density of (a) H_2 and (b) CO for pure Au, pure Pd, and all alloy compositions during CO2RR in 0.1 M $KHCO_3$ (pH = 6.8). The suppression of HER can be observed from the decrease in H_2 partial current density on icreasing the Pd content. The partial current densities of CO are also found to be higher for $Au_{75}Pd_{25}$ compared to Au, with $Au_{50}Pd_{50}$ also showing higher values than Au at low overpotentials.

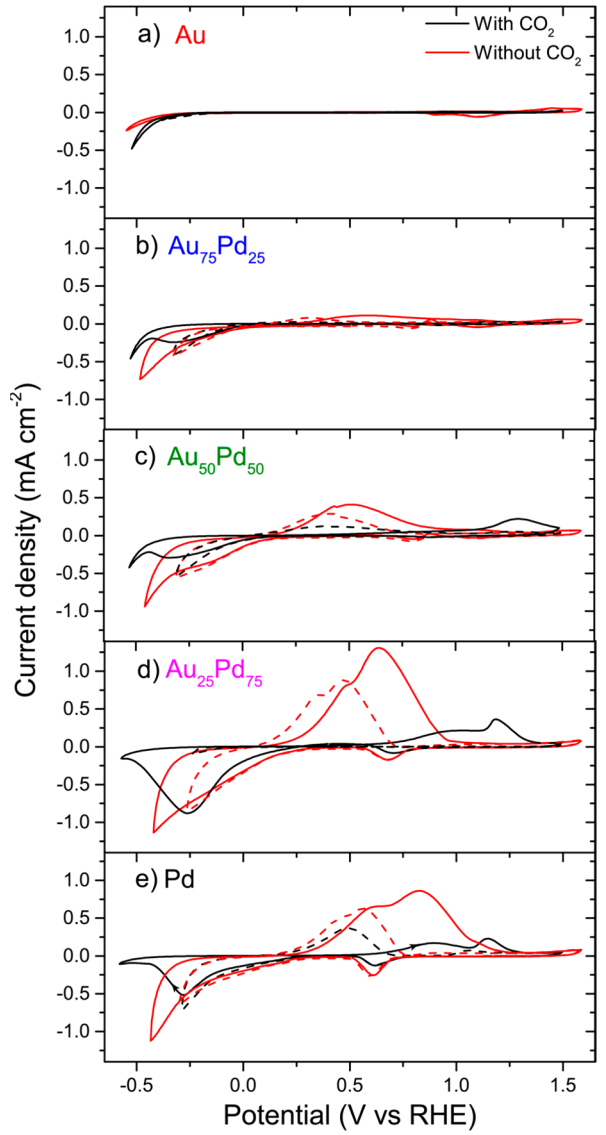

Figure 6. Long CV in the CO adsorption/desorption range (solid lines) and short CV in in the hydrogen adsorption/desorption range (dashed lines) of (a) Au, (b) $Au_{75}Pd_{25}$, (c) $Au_{50}Pd_{50}$, (d) $Au_{25}Pd_{75}$, and (e) Pd (solid lines) and short CV of Au, Pd, and Au−Pd alloys (dashed lines) taken in 0.1 M $KHCO_3$ with CO_2 (pH = 6.8, black) and without CO_2 (pH = 8.4, red) with a scan rate of 50 mV s^{-1}. Each cycle starts with a cathodic scan from 0.4 V to negative potentials (approximately −0.25 and −0.6 V) and then proceeds to 1.5 V. An anodic scan from 1.5 to 0.4 V follows.

from $Au_{75}Pd_{25}$ to $Au_{50}Pd_{50}$ (which also exhibits 100% FE for the competing reactions) could be explained by a decrease in the activity for the CO2RR due to a too strong binding energy with CO that hampers its release. However, to confirm this hypothesis that the main process responsible for the superior alloy FE for CO when compared with Au is the competition for active sites, we studied the voltammetric behaviors of the electrodes in the presence and absence of CO_2.

The CVs for all the synthesized electrodes with and without CO_2 purging at two different potential ranges (solid and dashed lines) are shown in Figure 6. For pure Au, the cathodic current at approximately −0.5 V vs RHE is larger when the electrolyte is saturated with CO_2 than when no CO_2 is purged. This can be explained by the fact that Au is not a good H_2 evolution catalyst[44] and, therefore, only a small HER current is developed without CO_2 purging. When CO_2 is present, an increased current is observed, which can be attributed to CO formation. On the other hand, for pure Pd at the same potential (i.e., approximately −0.5 V vs RHE), a much larger cathodic current is measured without CO_2 purging. This is expected because Pd is closer to the top of the volcano plot for the HER than Au.[42] However, an interesting observation for pure Pd is that, when CO_2 is present in the electrolyte, the current for H_2 evolution is significantly lowered. This phenomenon was already observed in Pd nanoparticles, and the authors claimed that the CO2RR species adsorb strongly to the Pd surface, limiting the HER sites and therefore suppressing the HER.[18] This explanation is in good agreement with the CV observations for the Pd electrode seen in Figure 6e. This figure shows a short-range CV (−0.25 V vs RHE to 1.5 V vs RHE, dashed black line) that only goes into the H absorption/adsorption region, revealing the position of the desorption peak for H in Pd. The same figure (Figure 6e) shows a long CV range (solid black line) that covers the adsorption region for both the H and CO2RR species at approximately −0.3 V vs RHE. In this long CV, only a CO desorption peak appears at ∼1.2 V vs RHE, indicating adsorption of CO2RR species at approximately −0.3 V vs RHE. Moreover, the fact that no H desorption peak was observed in the long-range CV is explained by a nearly complete coverage of the surface with CO2RR intermediate

DOI: 10.1021/acscatal.8b04604
ACS Catal. 2019, 9, 3527−3536

species that do not allow the absorbed H to desorb (see further evidence in the Supporting Information SI-6).

The suppression of the H_2 evolution reaction due to significant coverage of the Pd surface with CO_2 reduction species is in good agreement with the fact that H_2 evolution requires at least one proton to be adsorbed. The experimental data shown above indicate that the hydrogen-suppression mechanism, seen in Pd,[18] also occurs for all the AuPd alloy electrodes. Clearly, the CO_2 reduction intermediate species adsorption peak at approximately −0.3 V vs RHE is present for all the alloy electrodes (Figure 6). Moreover, the HER suppression effect is revealed by the lowering of the cathodic currents for all the alloys when CO_2 is introduced to the electrolyte (Figure 6). This HER suppression may be responsible for the superior FE for CO observed for all the alloy electrodes when compared with pure Au (Figures 3 and 4).

We explain this superior CO formation for the alloys by the fact that, when Pd is alloyed with Au, the alloy adsorbs the CO2RR intermediate species more strongly at lower potentials than pure Au, covering most of the alloy surface and, therefore, leaving significantly less sites for H adsorption. This effect hinders the HER because this reaction requires either one adsorbed proton (in the Heyrovsky step) or two adsorbed protons (in the Tafel step) to occur.[17] On the other hand, the adsorbed CO2RR species can react with water molecules from the electrolyte to form CO molecules, which can be more efficiently desorbed (than in pure Pd) due to the presence of Au in the alloy (i.e., weaker binding energies for CO than in pure Pd).

Even though the suppression of hydrogen evolution in pure Pd has been suggested before[18] due to similar voltammetric analysis as the one given above, in the present work in situ surface-enhanced infrared absorption spectroscopy (SEIRAS) measurements were carried out to confirm the HER suppression mechanism and identify the CO2RR adsorbed intermediate responsible for the high coverages. Cyclic voltammetry measurements (Figure 7a) were performed between −0.8 and 1.2 V vs RHE with a scan rate of 10 mV/s while simultaneously measuring with in situ SEIRA measurements (Figure 7b). Notably, sweeping in cathodic direction gave rise to a cathodic peak centered at approximately −0.2 V vs RHE (Figure 7a), which coincides very well with the initiation of bridge-bonded CO formation on the Pd surface inferred from the SEIRA spectra (Figure 7b). On the contrary to the expected vibrational Stark effect,[45] sweeping to more negative potentials exhibited a shift to higher wavenumbers in the CO band until −0.4 V vs RHE. This shift can be explained by dipole−dipole coupling between CO molecules at neighboring sites (please see section SI-9 in the Supporting Information for a full SEIRA analysis). This result is in agreement with corresponding experiments performed by applying a constant potential on the Pd electrode to exclude any effect of potential modulation while monitoring the frequency of the CO band (Figure 7c). In Figure 7c, the increase in the frequency of the CO bond clearly complies with the decrease in the current transient at approximately −0.3 V vs RHE. This strongly suggests that dense patches of interacting CO molecules are formed on the Pd surface under cathodic conditions in a short amount of time and are responsible for the decrease of current. This experiment (i.e., Figure 7c) not only confirms that the high coverages of CO2RR intermediates are responsible for the HER suppression but also identifies the main adsorbed intermediate as CO in the covered surface.

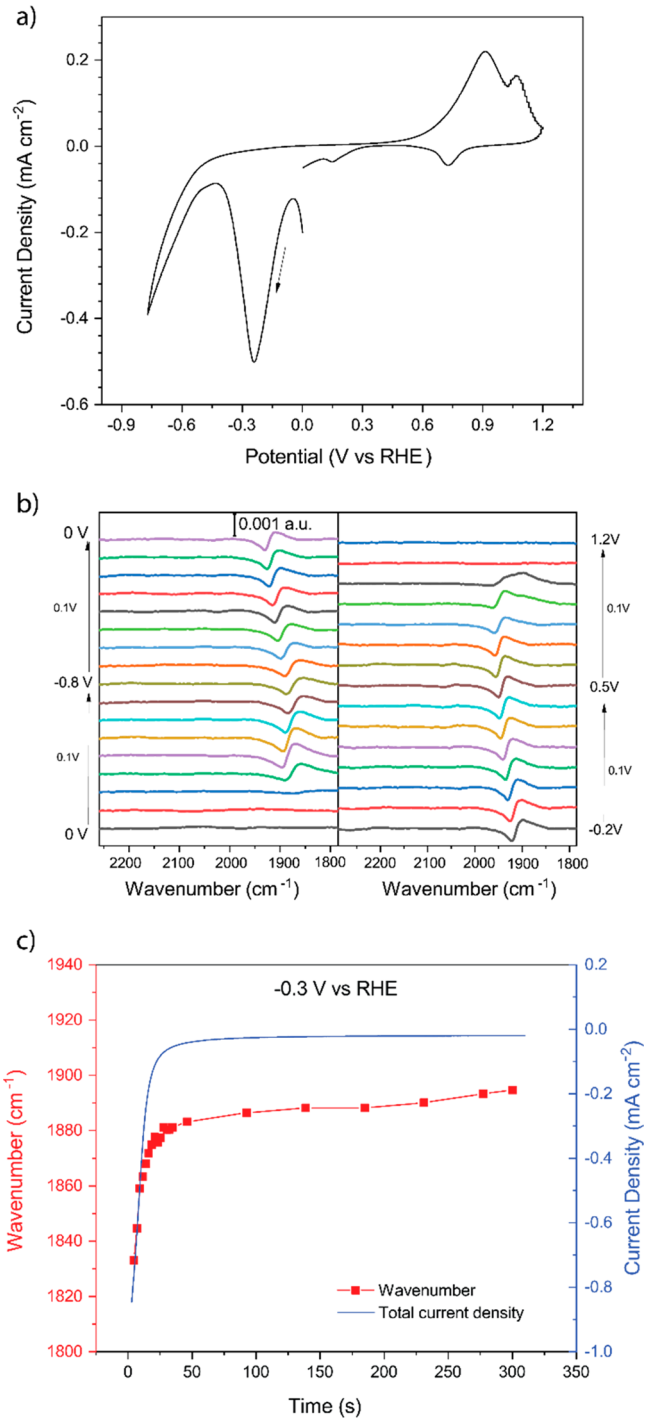

Figure 7. (a) Cyclic voltammetry curve of SEIRA active Pd thin films between −0.8 and 1.2 V in CO_2 saturated $KHCO_3$ solution. Scan rate: 10 mV/s. (b) Recorded in situ SEIRA spectra of adsorbed CO during the acquisition of the voltammetry curve. (c) Current transient of SEIRA active Pd films and peak center of CO peak at an applied potential of −0.3 V vs RHE in CO_2 saturated $KHCO_3$ solution.

DISCUSSION

These experiments not only confirm that high CO coverages are responsible for the suppression of the HER in pure Pd thin films but also show, for the first time, that the same HER

DOI: 10.1021/acscatal.8b04604
ACS Catal. 2019, 9, 3527−3536

suppression occurs for AuPd alloys with Pd concentrations as low as 25%. In this discussion we explain in detail, with the help of a kinetic model, the role of alloying Au with Pd in (i) enhancing the CO production at low overpotentials and (ii) suppressing the HER. Indeed, two main effects can be identified that can affect the selectivity toward CO in the Pd−Au alloys. The first effect is the change in the activity of the catalyst for the two competing reactions (i.e., CO2RR and HER). The activity depends on the binding energies of the intermediates involved in the mechanistic limiting step and the corresponding energy barrier. This way, the change in the measured FE of the catalysts with different alloy compositions obtained in this work (Figures 3 and 4) could be explained by an increase of the activity toward one of the competing reactions (e.g., due to more favorable binding energies). However, a second effect can be identified that can suppress a reaction (i.e., HER) despite the fact that the activity of that reaction can be improved. For example, if the set of HER and CO2RR reactions below are the only reactions occurring on the electrocatalysts and the RDS for the CO2RR is eq 5, it is expected for CO to accumulate on the surface, even at low applied potentials.

$$H_2O + e^- + * \overset{K_{vol}}{\longleftrightarrow} {}^*H + OH^- \quad (1)$$

$$^*H + H_2O + e^- \xrightarrow{k_{hey}} H_{2(g)} + OH^- + * \quad (2)$$

$$^*CO_2 + H_2O + e^- + * \overset{K_{CO2RR\_1}}{\longleftrightarrow} {}^*COOH + OH^- \quad (3)$$

$$^*COOH + H_2O + e^- \overset{K_{CO2RR\_2}}{\longleftrightarrow} {}^*CO + OH^- + H_2O \quad (4)$$

$$^*CO \xrightarrow{k_{CO2RR\_3}} CO_{(g)} + * \quad (5)$$

This is due to the fact that, with increasing applied potentials, the rate of the electrochemical CO_2 adsorption step (eq 3) increases (due to a continues decrease of the activation energy), while the rate of the nonelectrochemical desorption step (eq 5) is affected by the increasing potential to a lesser extent (e.g., through the potential-dependent coverage). This way, even if the activity for the HER of the alloy improves with Pd content, CO accumulation can selectively or randomly decrease the availability of active sites and suppress the HER.

This site competition can be better understood with the help of a simple kinetic model based on applying the pseudosteady-state approximation (PSSA) to the reactions considered above. The detailed description of the model is given in the Supporting Information (section SI-10). The model assumes that the rate-determining step (RDS) of pure Au for the CO2RR is the adsorption step (eq 3), as it is consistent with the literature.[20] This is confirmed by the fact that, as soon as the onset potential for adsorption is reached (cathodic onset in Figure 6a, approximately −0.38 V vs RHE), products are measured in the gas phase (the onset of CO partial currents on Au are between −0.35 and −0.4 V vs RHE in Figure 5b). However, for the Au-rich alloy, this observation changes drastically. When Au is alloyed with a relatively low amount of Pd (i.e., $Au_{75}Pd_{25}$), the current onset potential decreases 250 mV from approximately −0.35 to −0.1 V vs RHE (Figure 6b, black line). It is also observed that the Au-rich alloy has a peak around −0.25 V that is assigned to the adsorption of CO. Despite the fact that the surface is being populated with intermediate species at approximately −0.1 V vs RHE, the onset for the gas-phase CO product detection is measured only at approximately −0.35 V vs RHE (Figure 5b). This ∼250 mV difference between the onset potential for adsorption and the measurable release of CO is similar to the electrochemical behavior of Pd studied with in situ SEIRA shown earlier. Pd has a d-band much closer to the Fermi level than Au and binds much stronger with all the intermediates than Au, and thus, the RDS for the CO2RR is the release of CO. Therefore, the ∼250 mV difference between the CO_2 adsorption (approximately −0.1 V vs RHE, Figure 6b) and the CO release (approximately −0.35 V vs RHE, Figure 5b) observed in the Au-rich alloy suggests that the RDS of the alloy is not the adsorption reaction but the release of CO. Similarly, for alloys with higher Pd content, the model assumes the CO release as the RDS but with a larger activation energy barrier for the RDS with increasing Pd content.

The main purpose of the model is not to fit and estimate parameters but instead to understand the material- and potential-dependent trends of partial currents due to active site competition in order to validate and shed light into the proposed HER suppression, discovered earlier for the alloys. The coverages predicted by the PSSA model for the different alloys are shown in Figure 8.

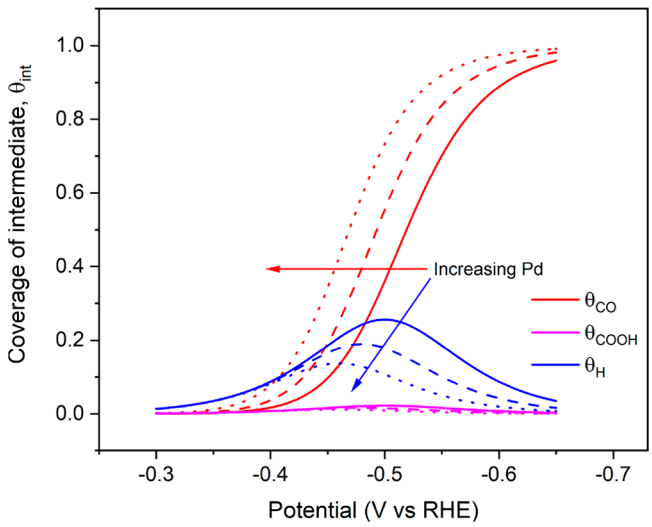

Figure 8. Potential- and material-dependent coverages of CO, COOH, and H on AuPd alloy electrodes as computed with the PSSA model. The solid, dashed, and dotted lines correspond to AuPd alloys with increasing Pd content, respectively.

Clearly, the CO coverage increases with potential, approaching 1 for potentials more negative than approximately −0.55 V vs RHE, while the coverages for H reach a maximum at approximately −0.5 V vs RHE. Accumulation of CO is expected at more negative potentials as long as the non-electrochemical CO desorption step is the RDS, because the reaction rate of the electrochemical Heyrovsky step increases with potential, allowing the H to be released as H_2 while the CO covers the surface. This ensures high CO coverages for all alloys and Pd. For Pd, the rate of CO release determined by the RDS is too slow and no significant CO release is measured at low overpotentials; for the alloys, the rate is expected to be greatly improved with the advantage (over pure gold) of (i)

DOI: 10.1021/acscatal.8b04604
ACS Catal. 2019, 9, 3527−3536

efficient adsorption at lower overpotentials and (ii) high coverages that can suppress the competing HER.

Figure 8 also shows that, by increasing the Pd content, high CO coverages are reached at lower overpotentials and the H coverages start decreasing also at lower applied potentials. Figure 9a shows the modeled partial current densities for the

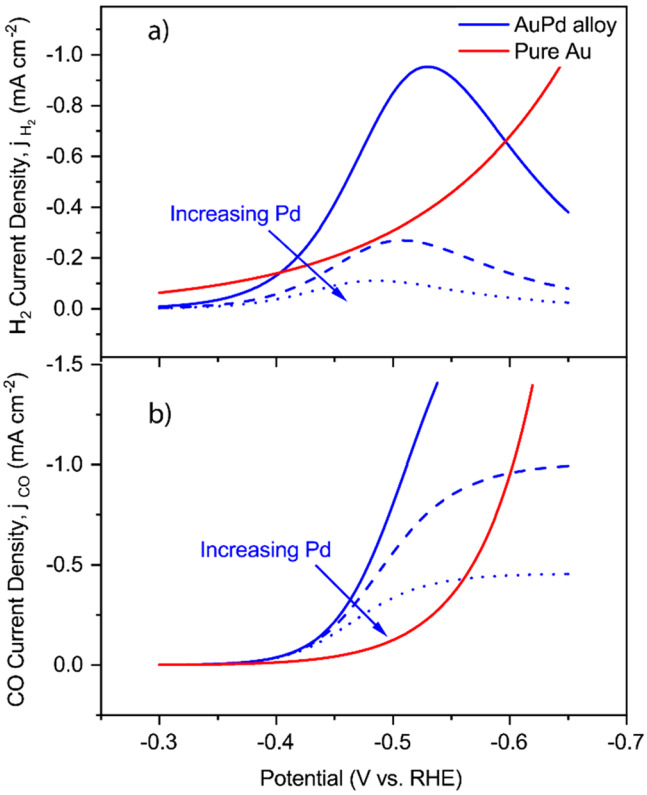

Figure 9. (a) H_2 and (b) CO potential- and material-dependent partial currents for AuPd alloy electrodes and a pure Au electrode as computed with the PSSA model. The blue solid, dashed, and dotted lines correspond to AuPd alloys with increasing Pd content.

HER. Interestingly, all the alloys show a decrease in the hydrogen partial current with increasing applied potential, precisely at the potential where the CO coverages are approaching 1 (i.e., approximately −0.55 V). This decrease in hydrogen partial current can be explained by the lack of available active sites for HER. This is in good agreement with our experimental observations, which show that the hydrogen partial currents decrease with increasing Pd composition (Figure 5a). Moreover, the modeled CO partial currents of the alloys, shown in Figure 9b, are clearly larger than the CO partial currents of pure Au at low overpotentials. The potential in which the partial current of Au surpasses the partial current of a specific alloy shifts to larger overpotentials with decreasing Pd content. This is in good agreement with the experimental data (i.e., Figure 5b), because pure Au starts overperforming $Au_{25}Pd_{75}$ at approximately −0.4 and $Au_{50}Pd_{50}$ at approximately −0.53 V vs RHE.

From comparing the PSSA model and experimental data, we conclude that the CO partial currents measured experimentally at low overpotentials are larger for the alloys than for Au due to (i) a significant ∼250 mV decrease of the CO_2 adsorption onset potential when compared with pure Au and (ii) the enhanced release of CO when compared with pure Pd. Moreover, the high selectivities are obtained due to the high CO coverages that decrease the availability of active sites for the HER.

An "ideal" alloy composition can be obtained depending on the desired gas product composition and applied potential. At low overpotentials AuPd alloys allow for higher CO generation and selectivity than pure Au. If the desired gas product needs to have a very low hydrogen composition, the Pd content of the catalyst can be increased and the HER suppression will be more pronounced (see Figures 5a and 9a). However, at a fixed potential there will always be a Pd composition threshold where the alloy starts producing less CO than Au (Figures 5b and 9b). Therefore, for a high concentration of Pd, high CO selectivity can come at the expense of less CO generation.

A possible explanation for the competition of sites resulting in such a strong HER suppression in AuPd could come from the fact that the adsorption of H on Pd is more favorable for highly coordinated sites (hollow sites),[46] which are significantly fewer in the heterogeneous $Au_{25}Pd_{75}$, $Au_{50}Pd_{50}$, and $Au_{75}Pd_{25}$ alloy surfaces than in the pure Pd surface; therefore, the site competition for these fewer sites can affect the selectivity even at overall low coverages.

Moreover, while the lack of hollow sites significantly hinders the adsorption of H, CO adsorption is not hindered because it can bind on top of Pd atoms.[47] This "single Pd active site" can explain the superior CO selectivity in the tested Au-rich alloy $Au_{75}Pd_{25}$ (when compared with pure Au) demonstrated in this work for applied potentials up to approximately −0.6 V vs RHE. This is because the single Pd sites in $Au_{75}Pd_{25}$ ensure (i) hindering of the HER (no hollow sites) and (ii) a favorable site competition for CO formation because the single Pd sites significantly favor CO adsorption.[47] This HER suppression based on the single Pd active site (separated by poor HER transition metals) was predicted by Karamad et al.[47] with DFT calculations. Those predictions[47] are in excellent agreement with our experimental findings. We conclude that the single Pd active sites in Au-rich AuPd alloys have enormous potential to achieve efficient and selective CO production.

It is clear from the kinetic model presented earlier that, as long as the CO release is the RDS for the alloys, Au will always surpass the alloys in CO generation at higher applied potentials because, unlike the CO release, the RDS of the pure Au electrode is an electrochemical step (i.e., CO_2 adsorption). Therefore, the alloys offer higher selectivity and generation rates of CO than Au only for low applied potentials. However, we expect interesting phenomena to occur in the alloy electrodes that are not captured by the model and can be engineered to allow the alloys to produce more CO at higher applied potentials than obtained in this work. One of these phenomena is the synergy between neighboring regions (in the atomic or nano scale) with differences in composition. These different regions within each alloy electrode were revealed by the CVs shown in Figure 2. Such regions with different compositions have different adsorption and desorption kinetics that can synergistically improve the overall CO2RR, while still maintaining high CO coverages and HER suppression. In this work we show that $Au_{75}Pd_{25}$ overperforms Au for CO generation up to, at least, approximately −0.6 V vs RHE.

This work shows that Au-rich Au−Pd alloys are excellent candidates to replace pure Au as the most active electrocatalyst for CO formation. To test their true potential, these Au-rich AuPd alloys should be tested in more efficient morphologies

DOI: 10.1021/acscatal.8b04604
ACS Catal. 2019, 9, 3527−3536

(e.g., nanoneedles) and more practical electrochemical cells (e.g., flow cells and gas diffusion electrodes).

■ ASSOCIATED CONTENT

Supporting Information

The Supporting Information is available free of charge on the ACS Publications website at DOI: 10.1021/acscatal.8b04604.

AFM, XPS valence band spectra before and after etching cycles, surface composition calculations using XPS, electrochemical CO_2 reduction, cyclic voltammetry and hydrogen adsorption calculations, ECSA calculation, XRD, in situ SEIRAS, and kinetic model (PDF)

■ AUTHOR INFORMATION

Corresponding Authors

*E-mail: Valenti@amolf.nl.
*E-mail: W.Smith@tudelft.nl.

ORCID

Marco Valenti: 0000-0002-0403-182X
Ming Ma: 0000-0003-3561-5710
Sixto Gimenez: 0000-0002-4522-3174
Bernard Dam: 0000-0002-8584-7336
Wilson A. Smith: 0000-0001-7757-5281

Notes

The authors declare no competing financial interest.

■ ACKNOWLEDGMENTS

Financial support from the VIDI project (granted to W.A.S.) by NWO is gratefully acknowledged.

■ REFERENCES

(1) Qiao, J.; Liu, Y.; Zhang, J. Electrochemical Reduction of Carbon Dioxide: Fundamentals and Technologies. *Electrochemical Energy Storage and Conversion*; CRC Press: 2016.

(2) Kim, D.; Resasco, J.; Yu, Y.; Asiri, A. M.; Yang, P. Synergistic Geometric and Electronic Effects for Electrochemical Reduction of Carbon Dioxide Using Gold−Copper Bimetallic Nanoparticles. *Nat. Commun.* **2014**, *5*, 4948.

(3) Kortlever, R.; Shen, J.; Schouten, K. J. P.; Calle-Vallejo, F.; Koper, M. T. M. Catalysts and Reaction Pathways for the Electrochemical Reduction of Carbon Dioxide. *J. Phys. Chem. Lett.* **2015**, *6* (20), 4073−4082.

(4) Humphrey, J. J. L.; Plana, D.; Celorrio, V.; Sadasivan, S.; Tooze, R. P.; Rodríguez, P.; Fermín, D. J. Electrochemical Reduction of Carbon Dioxide at Gold Palladium Core−Shell Nanoparticles: Product Distribution versus Shell Thickness. *ChemCatChem* **2016**, *8* (5), 952−960.

(5) Jovanov, Z. P.; Hansen, H. A.; Varela, A. S.; Malacrida, P.; Peterson, A. A.; Nørskov, J. K.; Stephens, I. E. L.; Chorkendorff, I. Opportunities and Challenges in the Electrocatalysis of CO_2 and CO Reduction Using Bifunctional Surfaces: A Theoretical and Experimental Study of Au−Cd Alloys. *J. Catal.* **2016**, *343*, 215−231.

(6) Hansen, H. A.; Shi, C.; Lausche, A. C.; Peterson, A. A.; Nørskov, J. K. Bifunctional Alloys for the Electroreduction of CO_2 and CO. *Phys. Chem. Chem. Phys.* **2016**, *18* (13), 9194−9201.

(7) Burdyny, T.; Smith, W. A. *Energy Environ. Sci.* **2019**, DOI: 10.1039/C8EE03134G.

(8) Hori, Y.; Wakebe, H.; Tsukamoto, T.; Koga, O. Electrocatalytic Process of CO Selectivity in Electrochemical Reduction of CO_2 at Metal Electrodes in Aqueous Media. *Electrochim. Acta* **1994**, *39* (11−12), 1833−1839.

(9) Liu, M.; Pang, Y.; Zhang, B.; De Luna, P.; Voznyy, O.; Xu, J.; Zheng, X.; Dinh, C. T.; Fan, F.; Cao, C.; De Arquer, F. P. G.; Safaei, T. S.; Mepham, A.; Klinkova, A.; Kumacheva, E.; Filleter, T.; Sinton, D.; Kelley, S. O.; Sargent, E. H. Enhanced Electrocatalytic CO_2 reduction via Field-Induced Reagent Concentration. *Nature* **2016**, *537* (7620), 382−386.

(10) Ma, M.; Djanashvili, K.; Smith, W. A. Selective Electrochemical Reduction of CO_2 to CO on CuO-Derived Cu Nanowires. *Phys. Chem. Chem. Phys.* **2015**, *17* (32), 20861−20867.

(11) He, J.; Johnson, N. J.; Huang, A.; Berlinguette, C. Electrocatalytic Alloys for CO_2 Reduction. *ChemSusChem* **2018**, *11*, 48−57.

(12) Sarfraz, S.; Garcia-Esparza, A. T.; Jedidi, A.; Cavallo, L.; Takanabe, K. Cu−Sn Bimetallic Catalyst for Selective Aqueous Electroreduction of CO_2 to CO. *ACS Catal.* **2016**, *6* (5), 2842−2851.

(13) Ma, M.; Hansen, H. A.; Valenti, M.; Wang, Z.; Cao, A.; Dong, M.; Smith, W. A. Electrochemical Reduction of CO_2 on Compositionally Variant Au-Pt Bimetallic Thin Films. *Nano Energy* **2017**, *42*, 51−57.

(14) Hori, Y. Electrochemical CO_2 Reduction on Metal Electrodes. In *Modern Aspects of Electrochemistry*; Vayenas, C. G., White, R. E., Gamboa-Aldeco, M. E., Eds.; Springer New York: New York, 2008; pp 89−189; DOI: 10.1007/978-0-387-49489-0_3.

(15) Hori, Y.; Murata, A.; Kikuchi, K.; Suzuki, S. Electrochemical Reduction of Carbon Dioxides to Carbon Monoxide at a Gold Electrode in Aqueous Potassium Hydrogen Carbonate. *J. Chem. Soc., Chem. Commun.* **1987**, No. 10, 728−729.

(16) Chen, Y.; Li, C. W.; Kanan, M. W. Aqueous CO_2 Reduction at Very Low Overpotential on Oxide-Derived Au Nanoparticles. *J. Am. Chem. Soc.* **2012**, *134* (49), 19969−19972.

(17) Zhang, Y. J.; Sethuraman, V.; Michalsky, R.; Peterson, A. A. Competition between CO_2 Reduction and H_2 Evolution on Transition-Metal Electrocatalysts. *ACS Catal.* **2014**, *4* (10), 3742−3748.

(18) Guo, R. H.; Liu, C. F.; Wei, T. C.; Hu, C. C. Electrochemical Behavior of CO_2 reduction on Palladium Nanoparticles: Dependence of Adsorbed CO on Electrode Potential. *Electrochem. Commun.* **2017**, *80* (April), 24−28.

(19) Shi, C.; Hansen, H. A.; Lausche, A. C.; Nørskov, J. K. Trends in Electrochemical CO_2 Reduction Activity for Open and Close-Packed Metal Surfaces. *Phys. Chem. Chem. Phys.* **2014**, *16* (10), 4720.

(20) Hansen, H. A.; Varley, J. B.; Peterson, A. A.; Nørskov, J. K. Understanding Trends in the Electrocatalytic Activity of Metals and Enzymes for CO_2 Reduction to CO. *J. Phys. Chem. Lett.* **2013**, *4* (3), 388−392.

(21) Gao, D.; Zhou, H.; Wang, J.; Miao, S.; Yang, F.; Wang, G.; Wang, J.; Bao, X. Size-Dependent Electrocatalytic Reduction of CO_2 over Pd Nanoparticles. *J. Am. Chem. Soc.* **2015**, *137* (13), 4288−4291.

(22) Wang, J. Y.; Zhang, H. X.; Jiang, K.; Cai, W. B. From HCOOH to CO at Pd Electrodes: A Surface-Enhanced Infrared Spectroscopy Study. *J. Am. Chem. Soc.* **2011**, *133* (38), 14876−14879.

(23) Jiang, K.; Zhang, H.-X.; Zou, S.; Cai, W.-B. Electrocatalysis of Formic Acid on Palladium and Platinum Surfaces: From Fundamental Mechanisms to Fuel Cell Applications. *Phys. Chem. Chem. Phys.* **2014**, *16* (38), 20360−20376.

(24) Nilsson, A.; Pettersson, L. G. M.; Hammer, B.; Bligaard, T.; Christensen, C. H.; Norskov, J. K. The Electronic Structure Effect in Heterogeneous Catalysis. *Catal. Lett.* **2005**, *100* (3−4), 111−114.

(25) Norskov, J. K.; Abild-Pedersen, F.; Studt, F.; Bligaard, T. Density Functional Theory in Surface Chemistry and Catalysis. *Proc. Natl. Acad. Sci. U. S. A.* **2011**, *108* (3), 937−943.

(26) Kortlever, R.; Peters, I.; Balemans, C.; Kas, R.; Kwon, Y.; Mul, G.; Koper, M. T. M. Palladium−gold Catalyst for the Electrochemical Reduction of CO_2 to C1−C5 Hydrocarbons. *Chem. Commun.* **2016**, *52* (52), 10229−10232.

(27) Hahn, C.; Abram, D. N.; Hansen, H. A.; Hatsukade, T.; Jackson, A.; Johnson, N. C.; Hellstern, T. R.; Kuhl, K. P.; Cave, E. R.; Feaster, J. T.; Jaramillo, T. F. Synthesis of Thin Film AuPd Alloys and Their Investigation for Electrocatalytic CO_2 Reduction. *J. Mater. Chem. A* **2015**, *3* (40), 20185−20194.

(28) Back, S.; Yeom, M. S.; Jung, Y. Understanding the Effects of Au Morphology on CO_2 Electrocatalysis. *J. Phys. Chem. C* **2018**, *122* (8), 4274−4280.

DOI: 10.1021/acscatal.8b04604
ACS Catal. 2019, 9, 3527−3536

(29) Hall, A. S.; Yoon, Y.; Wuttig, A.; Surendranath, Y. Mesostructure-Induced Selectivity in CO_2 Reduction Catalysis. *J. Am. Chem. Soc.* **2015**, *137* (47), 14834−14837.
(30) Nørskov, J. K.; Bligaard, T.; Rossmeisl, J.; Christensen, C. H. Towards the Computational Design of Solid Catalysts. *Nat. Chem.* **2009**, *1*, 37.
(31) Reske, R.; Duca, M.; Oezaslan, M.; Schouten, K. J. P.; Koper, M. T. M.; Strasser, P. Controlling Catalytic Selectivities during CO_2 Electroreduction on Thin Cu Metal Overlayers. *J. Phys. Chem. Lett.* **2013**, *4* (15), 2410−2413.
(32) Lowde, D. R.; Williams, J. O.; McNicol, B. D. The Characterisation of Catalyst Surfaces by Cyclic Voltammetry. *Appl. Surf. Sci.* **1978**, *1* (2), 215−240.
(33) Juodkazis, K.; Juodkazyte, J.; Sebeka, B.; Stalnionis, G.; Lukinskas, a. Anodic Dissolution of Palladium in Sulfuric Acid: An Electrochemical Quartz Crystal Microbalance Study *. *Russ. J. Electrochem.* **2003**, *39* (9), 954−959.
(34) Rand, D. A. J.; Woods, R. A Study of the Dissolution of Platinum, Palladium, Rhodium and Gold Electrodes in 1 m Sulphuric Acid by Cyclic Voltammetry. *J. Electroanal. Chem. Interfacial Electrochem.* **1972**, *35*, 209−213.
(35) Gossner, K.; Mizera, E. The Anodic Oxidation of Gold + Palladium Alloys. *J. Electroanal. Chem. Interfacial Electrochem.* **1982**, *140* (1), 47−56.
(36) Rand, D.; Woods, R. Determination of the Surface Composition of Smooth Noble Metal Alloys by Cyclic Voltammetry. *J. Electroanal. Chem. Interfacial Electrochem.* **1972**, *36*, 57−69.
(37) Łukaszewski, M.; Kuśmierczyk, K.; Kotowski, J.; Siwek, H.; Czerwiński, A. Electrosorption of Hydrogen into Palladium-Gold Alloys. *J. Solid State Electrochem.* **2003**, *7* (2), 69−76.
(38) Sluiter, M. H. F.; Colinet, C.; Pasturel, A. *Ab Initio* Calculation of the Phase Stability in Au-Pd and Ag-Pt Alloys. *Phys. Rev. B: Condens. Matter Mater. Phys.* **2006**, *73* (17), 174204.
(39) Rose, A.; Maniguet, S.; Mathew, R. J.; Slater, C.; Yao, J.; Russell, A. E. Hydride Phase Formation in Carbon Supported Palladium Nanoparticle Electrodes Investigated Using in Situ EXAFS and XRD. *Phys. Chem. Chem. Phys.* **2003**, *5* (15), 3220.
(40) Sheng, W.; Kattel, S.; Yao, S.; Yan, B.; Liang, Z.; Hawxhurst, C. J.; Wu, Q.; Chen, J. G. Electrochemical Reduction of CO_2 to Synthesis Gas with Controlled CO/H $_2$ Ratios. *Energy Environ. Sci.* **2017**, *10* (5), 1180−1185.
(41) Westerwaal, R. J.; Rooijmans, J. S. A.; Leclercq, L.; Gheorghe, D. G.; Radeva, T.; Mooij, L. P. A.; Mak, T.; Polak, L.; Slaman, M. J.; Dam, B.; Rasing, Th. Nanostructured Pd-Au Based Fiber Optic Sensors for Probing Hydrogen Concentrations in Gas Mixtures. *Int. J. Hydrogen Energy* **2013**, *38* (10), 4201−4212.
(42) Nørskov, J. K.; Bligaard, T.; Logadottir, A.; Kitchin, J. R.; Chen, J. G.; Pandelov, S.; Stimming, U. Trends in the Exchange Current for Hydrogen Evolution. *J. Electrochem. Soc.* **2005**, *152* (3), J23.
(43) Liu, X.; Xiao, J.; Peng, H.; Hong, X.; Chan, K.; Nørskov, J. K. Understanding Trends in Electrochemical Carbon Dioxide Reduction Rates. *Nat. Commun.* **2017**, *8*, 15438.
(44) Sheng, W.; Myint, M.; Chen, J. G.; Yan, Y. Correlating the Hydrogen Evolution Reaction Activity in Alkaline Electrolytes with the Hydrogen Binding Energy on Monometallic Surfaces. *Energy Environ. Sci.* **2013**, *6* (5), 1509.
(45) Wasileski, S. A.; Weaver, M. J. What Can We Learn about Electrode−chemisorbate Bonding Energetics from Vibrational Spectroscopy? An Assessment from Density Functional Theory. *Faraday Discuss.* **2002**, *121* (0), 285−300.
(46) Dong, W.; Ledentu, V.; Sautet, P.; Eichler, A.; Hafner, J. Hydrogen Adsorption on Palladium: A Comparative Theoretical Study of Different Surfaces. *Surf. Sci.* **1998**, *411* (1), 123−136.
(47) Karamad, M.; Tripkovic, V.; Rossmeisl, J. Intermetallic Alloys as CO Electroreduction Catalysts—Role of Isolated Active Sites. *ACS Catal.* **2014**, *4* (7), 2268−2273.

DOI: 10.1021/acscatal.8b04604
ACS Catal. 2019, 9, 3527−3536